Stable and Unstable Singularities in the Unforced Hele-Shaw Cell

Robert Almgren,*Andrea Bertozzi, †and Michael P. Brenner‡

December 6, 1995

Abstract

We study singularity formation in the lubrication model for the unforced Hele-Shaw system, describing the breaking in two of a fluid droplet confined between two narrowly spaced glass plates. By varying the initial data, we exhibit four different scenarios: (1) the droplet breaks in finite time, with two pinch points moving toward each other and merging at the singular time; (2) the droplet breaks in finite time, with two asymmetric pinch points propagating away from each other; (3) the droplet breaks in finite time, with a single symmetric pinch point; or (4) the droplet relaxes to a stable equilibrium shape without a finite time breakup. Each of the three singular scenarios has a self similar structure with different scaling laws; the first scenario has not been observed before in other Hele-Shaw studies. We demonstrate instabilities of the second and third scenarios, in which the solution changes its behavior at a thickness that can be arbitrarily small depending on the initial condition. These transitions can be identified by examining the structure of the solution in the intermediate scaling region.

*The University of Chicago, Department of Mathematics, 5734 S. University Ave., Chicago, IL 60637; almgren@math.uchicago.edu

†Mathematics and Computer Science Division, Argonne National Laboratory, 9700 S. Cass Avenue, Argonne, IL 60439, and Duke University, Department of Mathematics, Durham, NC 27708; bertozzi@math.duke.edu

‡To whom correspondence should be addressed; Department of Mathematics, MIT, Cambridge, MA 02139;brenner@math.mit.edu

1 Introduction

Singularity formation in physical systems, and in the partial differential equations that describe them, is a topic of great scientific interest. Breakdown of the mathematical model gives information on its limits, and extending the model often requires introduction of new and interesting physical ideas. Further, near the singularity, the solution often has a "universal" character, the same regardless of the initial conditions or the outer geometry. Thus by understanding the singularity, one obtains information about structural features of the model rather than specific predictions for a particular case. Singularities provide a unique "microscope" for understanding interesting systems.

One example is the breaking of a three-dimensional fluid drop into two pieces driven by the Rayleigh instability: breakup corresponds to singularity formation in the fluid velocity field. It has recently been shown that for breakup of an axisymmetric droplet in vacuum, the shape of the interface is described by a similarity solution [Egg93, ED94] which is unstable to finite amplitude perturbations [BSN94, SBN94]. The dynamics near the breaking point is completely independent of the outer flow field. This universality is a reflection of the fact that length and time scales near the pinch point are much smaller than any external scales near the breaking point. One might hope that this would be a general property of singularities in systems of interest, for example, velocity singularities in the three-dimensional Euler equations [Ker93, PS92, Maj86] or other singularities [CP93a].

A Hele-Shaw cell is a quasi two dimensional system in which two immiscible fluids (air and water) interact through their boundary in the narrow gap between two closely spaced glass plates. There are two types of stable equilibrium shapes for liquid trapped in this configuration: isolated circular drops [CP93b] and perfectly flat, infinitely long necks [BP95]. In the former case, the curvature on the interface is a positive constant; in the latter case, it is zero. For either equilibrium shape, interfaces close to equilibrium relax to the equilibrium state in infinite time. However, for initial shapes far from equilibrium, the end state is unclear. Will an initial shape that is topologically equivalent to an infinite thin neck but closely approximating an array of droplets relax to a flat infinite neck or will it break up into an array of droplets? If it breaks, how many satellite drops will form?

Note the important distinction between the present problem and the problem of a three-dimensional cylinder of fluid with surface tension controlling the liquid/air interface. Although the latter is unstable by the classical Rayleigh instability, a flat neck of liquid in the unforced Hele-Shaw cell is completely stable. However, it is still true that an initially perturbed neck in the Hele-Shaw cell has an infinite number of states, including the flat neck and various arrays of circular droplets. Whether the system chooses the flat neck or many droplets depends on whether there exist mechanisms that allow topology changes.

For breakup of a two-dimensional fluid droplet in a forced Hele-Shaw cell, several different types of local similarity solutions (with different scaling properties) can occur: an "infinite-time singularity" [CDG+93]; a finite-time singu-

larity in which the pinch point moves with constant velocity [DGKZ93]; and a finite-time singularity in which the pinch point is stationary [BBDK94, Ber95]. Varying the initial and boundary conditions leads to the different singular behaviors. Moreover, the same array of singularity structures is observed in a two-dimensional layer forced by density stratification in gravity [GPS93].

This paper addresses rupture of a thin neck in a Hele-Shaw cell in the absence of forcing. Based on the general principles of universality outlined above, one would expect that the local nature of singularities should be no different in the unforced case than in the forced case. However, our study reveals some qualitative features of the singularities that have not previously been observed in the forced case. Most strikingly, we discover through numerical simulations that two of the three similarity solutions can *destabilize* at an arbitrarily small time distance from the singularity for appropriate initial conditions. After the instability the solution develops a singularity at a later time, by a different similarity solution. We also find a new similarity solution that has never been observed in the forced Hele-Shaw cell. This mechanism appears to be more stable than the other two.

Our investigation of the unforced Hele-Shaw cell uses a one parameter family of initial conditions where the parameter w corresponds to the width of the "thread" connecting the larger drops in the initial interface shape. For sufficiently large w the "blobby" neck relaxes to a flat neck without breaking. However, for smaller values of w the neck tries to break up by a complex sequence of similarity solutions. In this paper, we discuss the scaling and stability of each of these solutions through highly resolved numerical simulations; many features of the simulations are explained through asymptotic analysis.

2 Review of Governing Equations

In a Hele-Shaw cell, a thin layer of viscous fluid moves between two narrowly spaced glass plates. Typically, the fluid does not fill the entire gap; the remaining space is filled by a fluid of negligible viscosity such as air. The fluid and the interface move under the influence of surface tension and a possible external forcing; viscosity in the fluid resists motion via the no-slip condition on the plate surfaces. The full system is described by the three-dimensional incompressible Navier-Stokes equations within the fluid layer, together with the Laplace pressure condition at the fluid/air interface, coupling the mean curvature of the interface surface with the pressure drop across the interface.

If the plate separation b is much smaller than any transverse dimension, then the well-known Hele-Shaw two-dimensional model system is a very good approximation. By Darcy's law, the depth-averaged fluid velocity $\mathbf{v}(x, y, t)$ is the gradient of a nondimensionalized velocity potential ϕ, proportional to negative pressure and defined in the two-dimensional fluid region. By incompressibility, ϕ is harmonic in x and y at each time: $\Delta\phi = 0$. The Laplace pressure condition becomes $\phi\big|_\Gamma = -\mathcal{K}$, in which $\mathcal{K}$ is the two-dimensional curvature of the fluid/air interface curve Γ. This Dirichlet problem is solved at each instant of time, and

material consistency requires that the interface normal velocity $V_n = \partial\phi/\partial n\big|_\Gamma$. For more details, see review articles such as [BKL$^+$86, KKL88].

We are interested in changes of topology in the *unforced* system. For example, we take a fluid droplet of finite size, surrounded by air, and ask whether for some initial shapes the droplet can break into two or more droplets. It has been proven [CP93b] that if the initial shape is close to a circle, then the droplet shape relaxes to a circle in infinite time. Recent numerical work [Alm96] indicates that if the initial droplet has the form of a dumbbell with a thin neck, it can break apart simply as a result of surface tension.

In the region of the thin neck, a lubrication approximation reduces the two-dimensional Hele-Shaw system to a one-dimensional model. We denote by $h(x,t)$ the half-width of the neck; then assuming that $|h_x| \ll 1$, and that $h \ll 1$ so that the pressure $p \approx p(x)$, yields the "lubrication equation" [CDG$^+$93]

$$h_t + (hh_{xxx})_x = 0. \tag{1}$$

This equation also follows from a systematic asymptotic expansion in h [Alm96, GPS93]. We are interested in the rupture of thin necks, when $h(x,t) \to 0$ in (1) at a finite time. In the lubrication model (2) the fourth-order term is *degenerate* and plays an interesting role in the formation of singularities. Simple reasoning [CDG$^+$93] shows that such vanishing of h requires that at least the fourth spatial derivative of h must become infinite; thus we are justified in calling such events singularities.

For circular droplets, the lubrication equation (1) is not uniformly valid over the whole liquid region; it breaks down where the ends close off. In [Alm96], the lubrication model was used in the center of the neck, with boundary conditions taken from an outer solution. The model can be extended to handle closed ends, as in [ED94] for three-dimensional liquid columns. Alternatively, special physical boundary conditions can force the entire neck to be thin and flat, as in [CDG$^+$93, DGKZ93].

To avoid these complications, we consider *periodic* geometry, rather than a closed finite drop. That is, in place of a dumbbell [Alm96], we consider an initial configuration in which the liquid forms an infinite sequence of bulges separated by thin necks. In order for the lubrication approximation to hold throughout the breaking of the neck, it must remain thin and flat for all time. We believe, and the numerical results of [Alm96] provide partial confirmation, that the local dynamics of the thin neck are the same in this geometry as for a closed droplet. In periodic geometry, the neck of constant thickness is a global attractor for the lubrication approximation [BP95].

Besides the intrinsic elegance and simplicity of the Hele-Shaw model, part of its appeal comes from the fact that the mathematical formulation describes several different physical problems, including solidification in the one-sided low-undercooling limit [KKL88] and population density in herbivore/plant dynamics [Lew94]. Thus, for example, the singularities studied here describe not only the pinching of a fluid neck in a Hele-Shaw cell, but also the singularities produced between two particles growing together in Ostwald ripening [VMBM88].

The approximations that permit reduction from the original problem to the two-dimensional, and then to the one-dimensional, model systems break down as the neck becomes very thin and the singularity is formed. Hence it is natural to question the relevance of the singularities studied here to the original problem. Based both on our asymptotic solutions near the singularity and numerical computations of the full equations [Alm96], the lubrication approximation, that is, the reduction of the two-dimensional Hele-Shaw system to the one-dimensional lubrication model, appears to remain valid as pinchoff occurs. However, the construction of the Hele-Shaw model itself breaks down when the neck width h becomes smaller than the plate spacing b due to the effect of the second component of curvature. We do not address this question in this paper, except for the few remarks in Section 7.

The lubrication equation (1) is naturally generalized to

$$h_t + (h^n h_{xxx})_x = 0, \tag{2}$$

in which $n = 1$ is the thin-neck limit of Hele-Shaw flow, and the case $n = 3$ is obtained from the dynamics of a thin liquid layer on a rigid surface. Varying n varies the nature of the degeneracy as $h \to 0$. The dynamics of solutions may then be explored as a function of n [BBDK94], and it appears that $n = 1$ is an especially difficult borderline case.

3 Simple Initial Data

This paper examines the behavior of solutions to Equation (1) with a one parameter family of initial conditions

$$h(x,0) = 1 - (1-w)\Big(1.5\,\cos \pi x \;-\; 0.6\,\cos 2\pi x \;+\; 0.1\,\cos 3\pi x \Big), \tag{3}$$

$w > 0$ (Figure 1). This data is periodic in x, and thus the solution $h(x,t)$ remains periodic. Alternatively, we could impose "neutral" boundary conditions $h_x = h_{xxx} = 0$ at the ends of a finite domain; in the Hele-Shaw system these conditions correspond to no transport of mass in or out of the domain and to normal contact angle.

We chose the initial data (3) to be completely smooth, with a single minimum of height w, at which the first four spatial derivatives of h vanish. These conditions produce an array of bulges with a very flat interconnecting regions of thickness w. The curvature takes a positive maximum value at $x = 1 - (1/\pi)\cos^{-1}(1/9) \approx 0.535$.

As a consequence of the above conditions, $h_{xxxx} > 0$ for x near to but greater than zero; hence, under the dynamics (1), $h_t < 0$ on the same region. Thus, at least for short times, the fourth-order dynamics will drive the neck thickness to decrease below its initial value. It is this mechanism that permits singularity formation, and that would be absent in a second-order equation.

We believe that the phenomena we observe in this paper for initial data (3) are generic, in the sense that they would be observed for a variety of initial

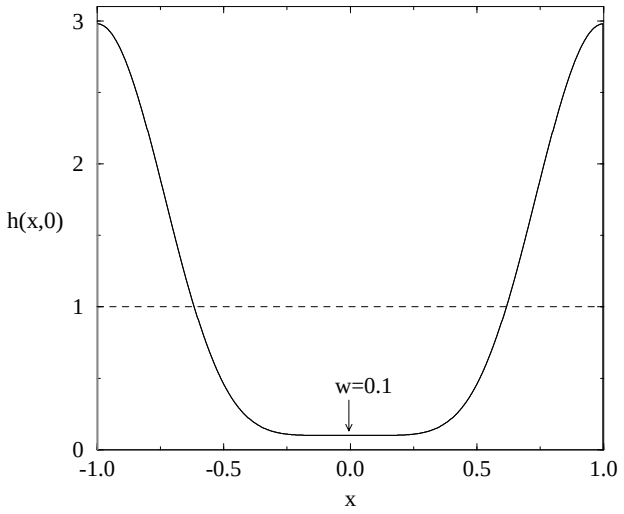

Figure 1: The initial condition (3) for parameter value $w = 0.1$. If no singularity forms in finite time, the solution must relax to its average $h = 1$.

conditions. It is necessary that the initial data be extremely flat; previous explorations with similar data containing only two Fourier modes exhibited no singularity.

Our numerical simulations use a finite-difference discretization [CDG+93] with a dynamically evolving adaptive mesh [BBDK94, Ber95]. The codes are well tested and can fully resolve many decades of behavior in the approach to the singularity.

Although the singularities have structures that locally have a simple self-similar form $h(x,t) \sim \tau(t) H((x - a(t))/\xi)$, the time dependent quantities τ and ξ cannot be determined by dimensional analysis. Moreover, unlike the typical scenario in such "second type" scaling [Bar79], the analysis of the similarity solution does not involve solving a nonlinear eigenvalue problem but instead involves solving matching conditions between different regions of the solution each of which has its own similarity scaling. It is this matching (or lack thereof) that we focus on in analyzing the instabilities described in the following sections. As w is varied, the simulations show several different possible behaviors of the solution, three of which lead to finite time singularities with these kind of well-defined self-similar scaling structures.

Imploding Singularity For initial conditions with $0 < w < w_1^* \approx 0.0665$, the solution developes two local minima that are mirror images of each other. They move towards each other at roughly constant speed, coalescing at $x = 0$

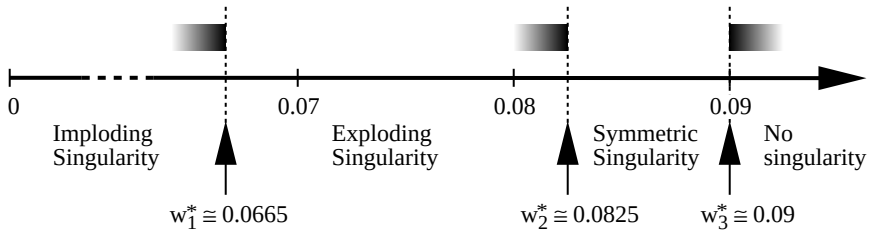

Figure 2: Phase diagram of singularity formation for solutions of (1) with initial data (3). The shaded bars indicate "instabilities": ranges of values of w in which the solution exhibits many decades of scaling characteristic of the neighboring singularity, before changing to the true singularity behavior.

at the singular time. This singularity is reported on for the first time here. The example exhibits three different scaling regions, the region around a local minimum, the central region between the two pinch points, and the outer region away from the singularity. We present a matching argument in the next section to predict the time dependences of the three regions.

Exploding Singularity For values of w greater than w_1^* but less than $w_2^* \approx 0.0825$, the solution developes two minima that move apart with roughly constant speed, with the pinchoff $h \to 0$ occurring at two locations $x = \pm x_*$. This behavior was first observed in [DGKZ93] for pressure boundary conditions. As discussed in that paper, this singularity has an inner self-similar region and an intermediate region. A consistent match between these two regions is necessary for the singularity to persist. We argue that the breakdown of this match is responsible for its destabiliation.

Symmetric Singularity For values of w greater than w_2^* but less than $w_3^* \approx 0.09$, a symmetric singularity forms: the solution is symmetric about a single minimum at $x = 0$, and $h(0,t) \to 0$. This solution was first discussed in [BBDK94] and later in [Ber95]. This behavior also possesses an intermediate length-scale.

No Singularity If the initial height w is not small, then the initial blobby neck simply relaxes to a constant flat neck as $t \to \infty$, as expected based on theoretical results [CP93b, BP95].
This behavior is summarized in the phase diagram of Figure 2.

The transitions between different singularity behaviors are more complicated than those found in previous studies. On one side of each critical parameter value, the solution appears to exhibit the neighboring behavior, showing clear self-similar scaling over many decades. However, at some critical neck thickness, the solution changes behavior into the true behavior for that parameter value. The neck thickness at which this transition occurs becomes arbitrarily small,

and the number of decades of deceptive self-similarity increases as the value of w moves closer to the critical value.

Thus, as illustrated in Figure 2, when w is just smaller than w_1^*, the solution initially exhibits the behavior characteristic of the "exploding singularity" until the minimum thickness h_{min} reaches a very small value h_{thresh}, at which the behavior changes to the imploding singularity. This changeover is seen dramatically in the fact that the distance between the two minima ceases to increase and starts to decrease. Similarly, for w just smaller than w_2^*, the symmetric singularity behavior is observed for many decades before the minimum bifurcates into two exploding singularities. For w just larger than w_3^*, the solution initially exhibits the features of the symmetric singularity, before reversing itself and rising toward the uniform state.

The evidence for our arguments is based only on numerical simulation; hence we cannot exclude the possibility that further surprises occur at even thinner neck widths. However, a major point of this paper is identification of the *differences* between the deceptive self-similar behavior and the ultimate singularity structure that emerges upon enhanced resolution. In many instances, the only observed difference between an apparently stable structure and an unstable one is that of different behavior in the intermediate matching regions. A remaining major challenge is to construct a general explanation of why these different scalings ultimately destabilize.

In the following three sections, we discuss each of the finite-time singularity mechanisms. In Section 4 we present numerical evidence for the "imploding" singularity mechanism and derive a similarity solution that reproduces its scaling properties. We have never observed instability of this solution and transition to a different behavior.

In Section 5, we discuss the "exploding" singularity and generalize the known similarity solution [DGKZ93] to a one-parameter family of solutions with different scaling exponents. Three members of this family appear in our calculations: (a) the solution of [DGKZ93], with pinch points moving apart at a constant velocity; (b) a solution with accelerating pinch points; (c) a solution with decelerating pinch points. The latter two cases apparently suffer an instability at a finite (but arbitrarily small, depending on initial data) neck thickness. We provide a partial explanation of the instability of the new members of this family, based on a mismatch in velocities between the intermediate regions on the two sides.

In Section 6 we discuss the symmetric singularity mechanism. Here we distinguish between two types of solution, only one of which appears to be stable, and we provide a partial explanation of the destabilization and transition to the exploding singularity.

4 Imploding Singularity

In this section we discuss numerical observations and a scaling analysis for the imploding singularity.

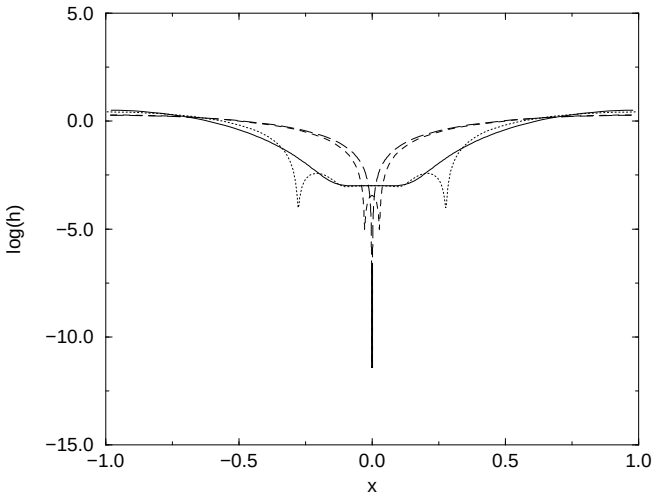

Figure 3: Imploding singularity at $w = 0.01$. The solid, dotted, dashed and long dashed curves correspond to times $t = 0, 3.3, 3.4, 3.9 \times 10^{-3}$ respectively.

4.1 Numerical Observation and Scaling Relationships

When the initial minimum thickness w is very small, the solution approaches a singularity in which two pinch points propagate toward each other, merging at the singular time. This is a new type of singularity; it has not been seen in the forced geometry and is reported here for the first time. Figure 3 illustrates this behavior for $w = 0.01$.

The initial condition, with a single local minimum, bifurcates into two minima, which then propagate toward the origin, merging at the singular time. Several nontrivial scaling laws are associated with this singular behavior. Figure 4 shows the height at the pinch points, $h_{min}(t)$, as a function of their position $\pm x_{min}(t)$. As the thickness approaches zero, $h_{min}(t) \to 0$, the pinch points propagate toward the origin, $\pm x_{min}(t) \to 0$. The data is consistent with the scaling law

$$h_{min} \sim x_{min}^6.$$

Another relevant quantity is $h(0) = h(0,t)$, the thickness of the interface at the center $x = 0$. As the pinch points propagate toward the origin, mass flows away from the neighborhood of the origin, so that $h(0)$ decreases. Figure 4 also shows $h(0)$ as a function of the pinch location $x_{min}(t)$. The data is consistent with the scaling law

$$h(0) \sim x_{min}^3.$$

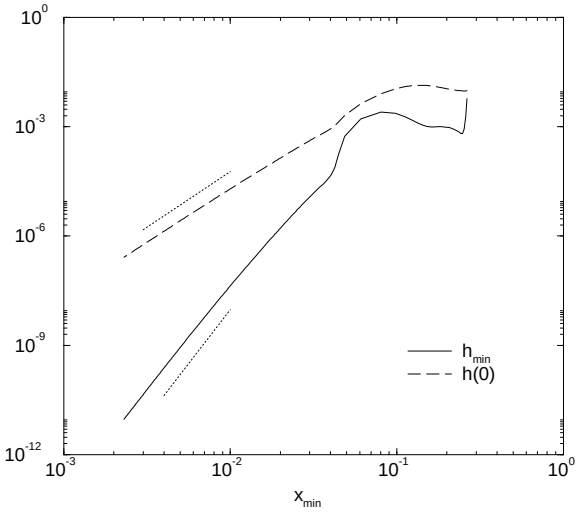

Figure 4: Minimum position x_{min} vs. minimum thickness h_{min}, and thickness at origin $h(0)$ for the imploding singularity of Figure 3. The uppermost dotted line represents the scaling law $h(0) \sim x_{min}^3$, while the lowermost dotted line represents the scaling law $h_{min} \sim x_{min}^6$.

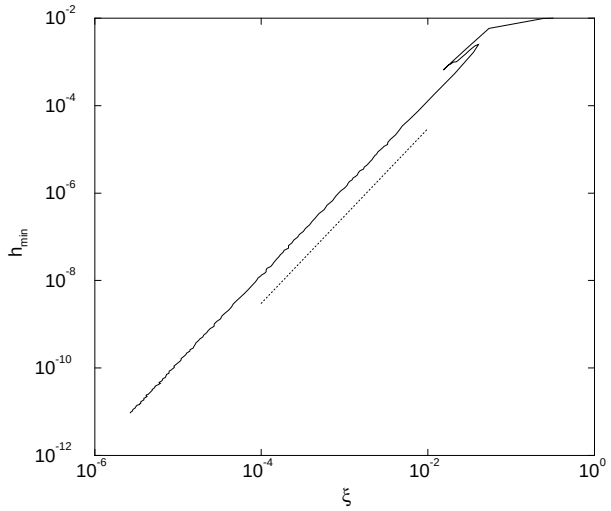

Figure 5: Pinch length scale ξ vs. minimum thickness h_{min}, for the imploding singularity of Figure 3. The dotted line represents the scaling law $h_{min} \sim \xi^2$.

The final relevant scaling law is the characteristic width ξ around the pinch point as a function of h_{min}. As we determine by the explicit construction below, the singularity has a locally parabolic structure, so that

$$h_{min} \sim \xi^2, \tag{4}$$

as verified in Figure 5.

4.2 Construction of Similarity Solution

Now we construct a one-parameter family of similarity solutions to equation (1). At a special value of this parameter the similarity solution well describes the behavior presented above, both in explaining the scaling laws and in predicting the shape of the interface close to the singular time. The singularity has three different self-similar scaling regions, which we call the central region, the pinch region, and the outer region. The scaling exponents, and hence the time dependence, are determined by requiring that the solutions in the three regions match. The construction is similar in spirit to the description of the infinite-time singularity in the forced Hele-Shaw cell [CDG$^+$93]. We proceed by first describing the solution in each region separately, and then matching them together to determine the scaling exponents.

4.2.1 Central Region

In the central region, we look for an exact similarity solution of the form

$$h(x,t) = \tau(t)\, S\left(\frac{x}{\tau(t)^q}\right), \tag{5}$$

in which the time dependence $\tau(t)$, the profile function $S(\eta)$, and the exponent q are to be determined; here $\eta = x/\tau^q$ denotes the similarity variable. Substituting (5) into (1), and then separating the t and η dependences, gives the two equations

$$\dot{\tau} = -\tau^{2-4q} \tag{6}$$

and

$$S - q\eta S' = (SS''')'. \tag{7}$$

Equation (6) implies that

$$\tau(t) \propto (t_c - t)^{1/(4q-1)}$$

whenever $q > 1/4$. This is an example of an exact similarity solution to the equation. Although it describes well the structure in the center of the imploding singularity profile, such an exact solution has not been observed in the pinch region of a singularity of the lubrication equation (2) for any n. It is not known whether such a solution exists for *any* q.

Solutions to (7) that describe the central region are known to exist and are compactly supported in η. These solutions satisfy the symmetry conditions

$$S(0) = 1, \qquad S'(0) = S'''(0) = 0.$$

If we consider all such solutions to (7) with $S''(0) = c$, when c is large, the solution is compactly supported on $(-\eta_0, \eta_0)$ with $S(\eta) \sim \eta_0 - \eta$ near $S(\eta_0) = 0$. These solutions are undesirable because they cannot be matched to the other regions. However, there is a unique critical value $c = c_0(q)$ such that the solution touches down like $S(\eta) \sim (\eta_0 - \eta)^{3/2}$ It is easy to construct such a solution numerically for any q by using a shooting method. Notice that, since SS''' has a finite positive limit at η_0, a nonzero flux of fluid leaves the central region.

4.2.2 Pinch Region

In the pinch region around $\pm x_{min}$, our numerical evidence indicates that the current $J(t)$ is constant, so that we can write

$$hh_{xxx} = J(t).$$

This is consistent with the numerical and asymptotic studies of the infinite-time [CDG+93] and the finite-time [DGKZ93] singularities in the forced geometry. As

described in detail in those references, this suggests that the pinch region may be described by a scaling solution that to leading order, satisfies the constant flux equation (that is, the time derivative h_t is lower order than the flux term $(hh_{xxx})_x$ in the PDE. We look for solutions with the self-similar form $h(x,t) = \alpha(t)\, H(x/\alpha^p)$. With the special choice $\alpha(t) = J(t)^{1/(2-3p)}$, we have the time-independent equation for the similarity spatial profile H

$$HH''' = 1. \tag{8}$$

Equation (8) has special solutions with [CDG+93]

$$H(\eta) \sim \begin{cases} \frac{1}{2}\eta^2, & \eta \to \infty, \\ \sqrt{\frac{8}{3}}\,(A-\eta)^{3/2}, & \eta \to -\infty, \end{cases}$$

where A is an arbitrary constant. The time dependence $\alpha(t)$, or equivalently the current $J(t)$, are determined by matching this solution to the central and outer solutions.

4.2.3 Outer Region

In the outer region, the solution is of the form $h(x,t) = K(x - a(t))$, where $a = x_{min}$ is the location of the minimum. Plugging into equation (1) gives

$$\dot{a}K = KK''' + C(t).$$

The relevant solution has the pinch region moving at constant velocity $\dot{a} = U$, and also $C = 0$ independent of time. The solution is

$$K(y) = \tfrac{1}{6}Uy^3 + Ay^2 + By,$$

where A and B are arbitrary constants.

4.2.4 Matching Conditions

To complete the solutions it is necessary to match the three regions together. There are matching conditions connecting the pinch region to both the outer region and the central region. For the pinch solution to match onto the outer solution, we require

$$\lim_{\eta\to\infty} \alpha(t)\, H(\eta) = \lim_{y\to 0} K(y).$$

This matching condition requires that both the time dependences and the spatial dependences balance. This balance is achieved by taking $H(\eta) \sim A\eta^2$ as $\eta \to \infty$ and $p = 1/2$, for the pinch solution, and taking $B = 0$ for the outer solution. Also, the pinch solution must move at the velocity dictated by the outer solution.

Matching the pinch solution onto the central solution requires that

$$\lim_{\eta\to-\infty} \alpha(t)\, H(\eta) = \lim_{S\to 0} \tau\, S\left(\frac{x}{\tau^q}\right).$$

This condition can be satisfied by taking $H(\eta) \sim |\eta|^{3/2}$ as $\eta \to -\infty$. Also, for the time dependences to match, the flux of fluid leaving the central region must enter the pinch region. The flux leaving the central region is of order

$$\tau^{2-3q} \sim (t_c - t)^{(2-3q)/(4q-1)}.$$

The flux entering the pinch region is of order $\alpha^{1/2}$. Thus we have the scaling law

$$\alpha \sim \tau^{4-6q} \sim (t_c - t)^{(4-6q)/(4q-1)}.$$

Finally, note that the minimum point moves toward the origin $x = 0$ with velocity $(t_c - t)^{(3q-1)/(4q-1)}$. Demanding that the outer edge of the central region moves with the same *constant* velocity as the inner edge of the outer region fixes $q = 1/3$.

Putting these conditions together give the scaling laws

$$\begin{aligned} h_{min}(t) &\sim x_{min}^6 \\ h(0) &\sim x_{min}^3 \\ h_{min} &\sim \xi^2 \\ x_{min} &\sim t_c - t. \end{aligned}$$

These scaling laws agree quite well with the evidence from the numerics.

5 Exploding Singularity

For larger values of w, solutions approach a singularity in which there are two minimum points that move *away* from each other as the singularity approaches. An example of an exploding singularity is shown in Figure 6 for the initial condition $w = 0.07$.

At early times the minimum thickness is at $x = 0$. This single minimum then bifurcates into two minima, which propagate away from each other, forming simultaneous singularities at $\pm x$. Several different scaling laws are associated with this singularity. Figure 7 shows the characteristic length scale ξ, defined as the distance over which the thickness of the interface doubles, as a function of the minimum thickness h_{min}.

This type of singularity was first discussed by [DGKZ93], in the context of a thin neck squeezed by external pressure. It is also readily observed when fluid is drained from the neck at a constant rate [BBDK94] or when the thin neck is forced by Rayleigh-Taylor instability [GPS93, GPS95]. For details the reader is referred to the above references.

A theory for this type of singularity was first proposed by [DGKZ93]. Below we summarize the major features of the solution; our derivation is slightly simpler and correspondingly less rigorous than that of [DGKZ93]. Our purpose is to expose the main features of the theoretical solution in order to extend the solution to treat new phenomena in the next section.

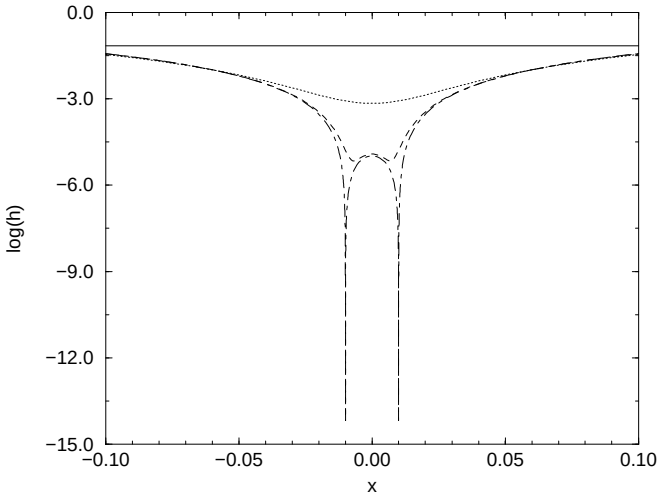

Figure 6: Exploding singularity at $w = 0.07$. The solid, dotted, and dot-dashed curves correspond to times $t = 0,\ 2,\ 2.4,\ 2.422\ \times 10^{-3}$, respectively, corresponding to a singularity at $x \approx 0.01$.

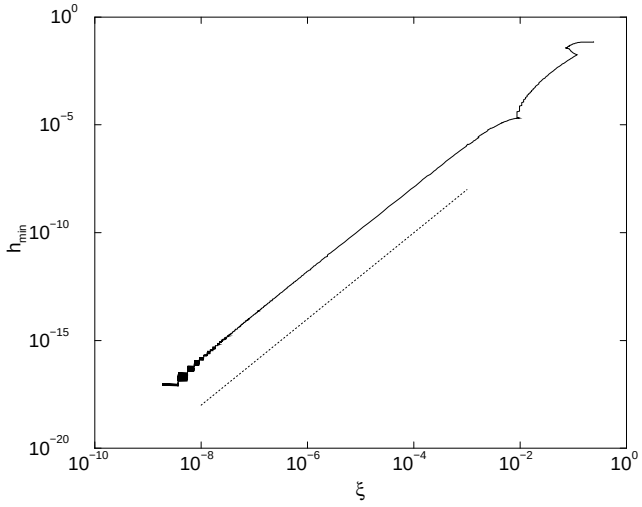

Figure 7: Minimum thickness h_{min} as a function of pinch length scale ξ, for the stable exploding singularity of Figure 6. The dotted line shows the theoretical prediction $h_{min} \sim \xi^2$.

Three separate scaling regions are present, the pinch region (local minimum), the intermediate region, and the outer region. In the pinch region the solution obeys

$$hh_{xxx} = J(t),$$

so that very close to the singularity the current does not depend on space. Taking

$$h(x,t) = \xi^2 \, H\left(\frac{x-a}{\xi}\right)$$

gives

$$H H''' = 1 \tag{9}$$

and $\xi = J$. Here $a(t)$ is the position of the pinch point.

As in the case of the previous example of the "imploding" singularity, the solution in the pinch region does not determine the time dependence of ξ. This time dependence results from a match to an intermediate region. The solution $H(\eta)$ to (9) has $H(\eta) \sim \eta^2$ as $\eta \to \infty$ [BKO93], or equivalently $h(x,t) \sim (x-a)^2$. Since this behavior is independent of ξ, it cannot determine the time dependence of ξ. Thus we must analyze lower-order terms. A little algebra shows that

$$h(x,t) = A(x-a)^2 + \xi(x-a)\log\frac{x-a}{\xi} + \ldots \, . \tag{10}$$

The second-largest term in the expansion must be matched to an intermediate region.

The intermediate region has the leading order asymptotic behavior $(x-a)^2$ of the pinch region; that is, in the intermediate region, h has the form

$$h(x,t) = A(x-a)^2 + g(x,t). \tag{11}$$

For the singularity to occur in finite time, g must vanish in finite time.

We find the time dependence of g by looking for a similarity solution

$$g(x,t) = \ell^r \, G\left(\frac{x-a}{\ell}\right), \tag{12}$$

where $\ell(t)$ is an intermediate length scale, and the similarity variable is $\zeta = (x-a)/\ell$. Plugging (11) and (12) into the original equation (1) gives

$$\dot{\ell}\ell^{r-1}(rG - \zeta G') - \ell^{r-1}\dot{a}G' - 2A\dot{a}\ell\zeta \\ + A\ell^{r-2}(\zeta^2 G''')' + \ell^{2r-4}(GG''')' = 0. \tag{13}$$

We determine the asymptotic behavior of both $G(\zeta)$ and $\ell(t)$ by first identifying leading terms in (13), and then separating t and ζ dependence.

The balance chosen by [DGKZ93] takes $r = 3$, and

$$\dot{a} = \text{constant} \quad \text{and} \quad \ell(t) \sim (t_c - t)^{1/2}. \tag{14}$$

Then the leading-order terms of (13) for $\ell \ll 1$, that is, for $t \to t_c$, give the ordinary differential equation for $G(\zeta)$

$$-\tfrac{1}{2}(3G - \zeta G') + A(\zeta^2 G''')' - 2A\zeta = 0. \tag{15}$$

Solutions to (15) have $G(\zeta) \sim \zeta$ for small ζ.

Asymptotic matching requires that the small-ζ behavior of the intermediate solution agree with the large-η behavior of the pinch solution (10). That is, we must have

$$\ell^2 (x - a) \sim \xi (x - a) \log \frac{\ell}{\xi}$$

or

$$\xi \sim \frac{\ell^2}{\log \frac{\ell}{\xi}} \sim \frac{(t_c - t)}{\log(t_c - t)}.$$

Thus, the decay of the intermediate region to a parabola determines the time dependent scales in the pinch region. Note that an implicit assumption of these scaling laws is that the intermediate regions on both sides of each minima have the same time dependences. This is tested and shown to be true in Figure 8. However, we will see in the next section that this assumption sometimes breaks down, causing instabilities in the similarity solution.

For the simulation shown above, we can indeed see the nontrivial scaling of the intermediate region. Figure 8 shows the length scale ℓ of the intermediate region as a function of the minimum thickness h_{min}. Notice that before the asymptotic behavior $h_{min} \sim \ell^4$ sets in, there is a transient behavior in which only the inner side (smaller $|x|$) of the pinch regions satisfies the scaling law $h_{min} \sim \ell^3$. At the thickness $h_{min} \approx 10^{-10}$ there is a crossover in which (a) both the outer (larger $|x|$) intermediate regions and the inner intermediate regions obey the same scaling law, and (b) the scaling law agrees with that proposed in [DGKZ93]. The behavior occurring before the crossover is interesting and is discussed in the next section. Note that Figure 7 showing the dependence of h_{min} on ξ shows no evidence of this crossover.

Instability of the Exploding Singularity

Different initial conditions from those of the preceding section lead to an exploding singularity that destabilizes, even after arbitrarily many decades of scaling (the precise number depending on initial conditions). To illustrate this instability (which was never observed in simulations of the forced Hele-Shaw cell, or in Figure 8), we condition the initial condition with $w = 0.0662$. At early times the solution mimics the behavior shown in the previous example: the solution

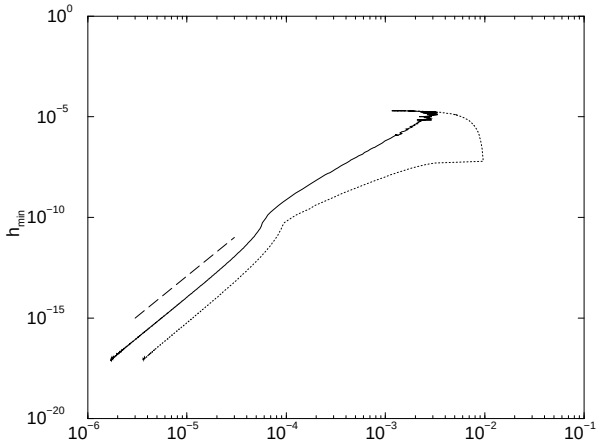

Figure 8: Intermediate length scale ℓ as a function of minimum thickness h_{min}, for the stable exploding singularity of Figure 6: solid line, measured on the outer side of the pinch points (larger x); dotted line, measured on the inner side of the pinch points (smaller x). The dashed line shows the theoretical prediction $h_{min} \sim \ell^4$.

falls slightly in the center with two minima that propagate outward, attempting to break at the points $x_{min} \approx \pm 0.016$.

The solution in the pinch region follows the exploding behavior for many decades: Figure 10 show the scaling laws for the characteristic length scale in the pinch region, defined as the length scale over which the thickness doubles. There is a large range of scales where the scaling behavior coincides with that of the exploding singularity.

However, the data in the intermediate region tells a different story. Figure 11 shows $h_{min}(t)$ versus ℓ for the present case. The solid line corresponds to the measurement of ℓ on the inside of the pinch points. The dotted line corresponds to a measurement of ℓ on the outside of the pinch points. The upper long-dashed straight line corresponds to the law $h_{min} \sim \ell^3$; the lower dashed straight line corresponds to the scaling law $h_{min} \sim \ell^6$. This plot has several important features: At $h_{min} \sim 10^{-6}$, the outside intermediate scale begins to follow the same $h_{min} \sim \ell^3$ law noted above for early times. However, in this regime, the inside intermediate scale does not satisfy any noticeable scaling law. At a length scale of approximately 10^{-10}, there is a transition in both the inner and outer intermediate regions. Beyond this transition, the outer intermediate region seems to obey the scaling law $h_{min} \sim \ell^6$; however, the inner intermediate region displays a sharper dependence, consistent with $h_{min} \sim \ell^7$.

This behavior in the intermediate region has an important consequence, as

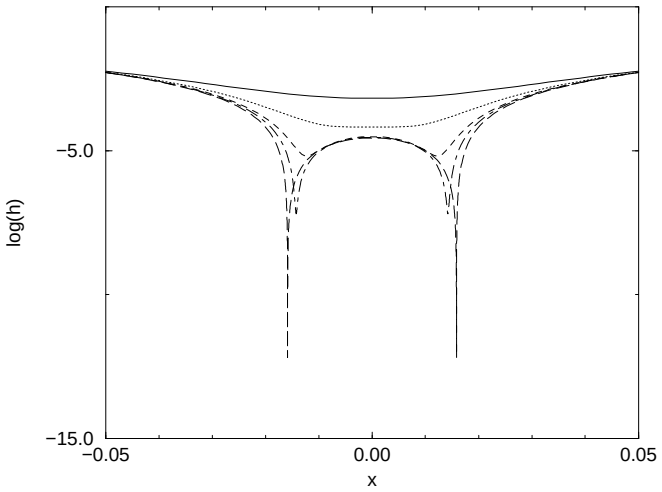

Figure 9: Approach to exploding similarity solution for $w = 0.0662$ at early times. The solid, dotted, dashed, and dot-dashed lines correspond to times $t = 2.3, 2.42, 2.427, 2.43 \times 10^{-2}$, respectively,i seemingly leading to a finite time singularity at $x = \pm 0.016$.

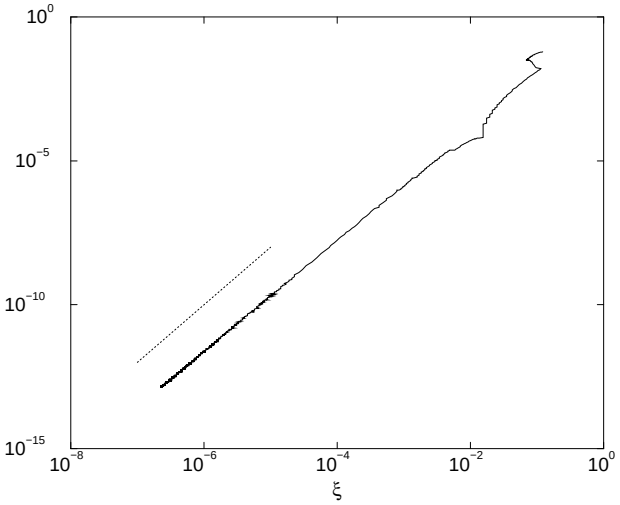

Figure 10: Pinch length scale ξ as a function of minimum thickness h_{min}, for the unstable exploding singularity of Figure 9. The dotted line shows the theoretical prediction $h_{min} \sim \xi^2$.

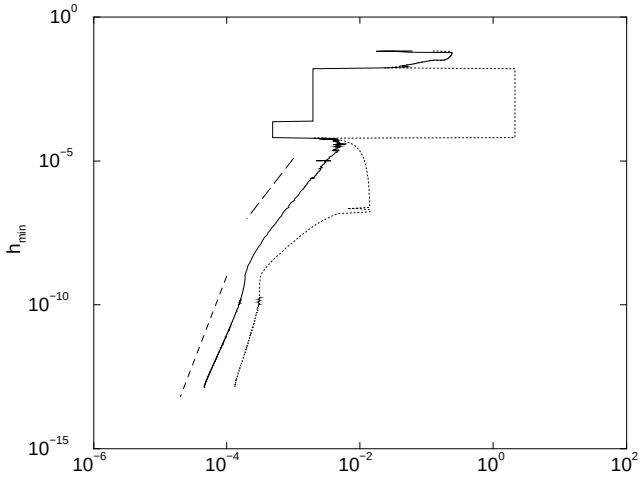

Figure 11: Intermediate length scale ℓ as a function of h_{min}, for the unstable exploding solution of Figure 9: dotted curve, measured on the inside of the singularity; solid curve, measured on the outside. The upper dashed line corresponds to $h_{min} \sim \ell^4$, the lower dashed line to $h_{min} \sim \ell^6$.

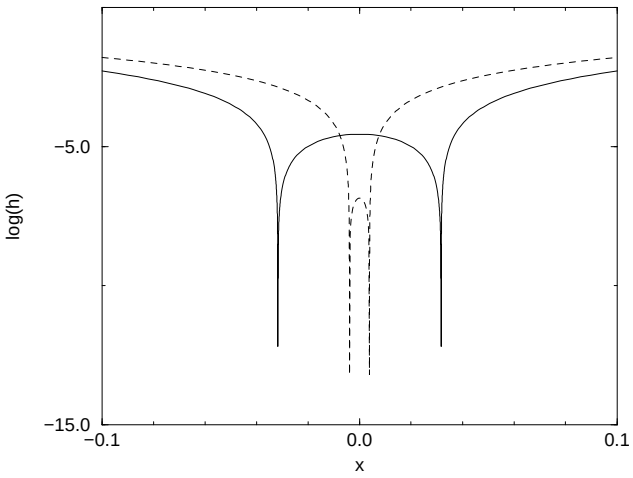

Figure 12: Transition behavior for $w = 0.0662$, for times following those of Figure 9: solid line, $t = 0.00243$; dashed line, $t = 0.0032$. The nature of the solution has changed dramatically, even at this extremely short time before the (failed) singularity.

now shown: continuing the simulation beyond the last time shown in the previous figures (when $h_{min} \sim 10^{-13}$), the behavior changes dramatically. Figure 12 shows the minimum thickness immediately after Figure 9.

The temporal behavior of the solution is demonstrated by plotting the logarithm of h_{min} versus the logarithm of $|x_{min}|$, the distance from the origin of the location of the minima (Figure 13). Beyond the critical thickness $h_{min} \sim 10^{-13}$ the minima turn around and propagate toward the origin. After turning around, the solution approaches the new singularity mechanism, the *imploding singularity*, discussed in the preceding section.

A potential source of the deviation in intermediate region from the scaling solution discussed in the preceding section lies in the velocity $\dot{a}$ of the pinch points. Figure 14 shows this velocity as a function of the minimum thickness, h_{min}.

At early times (corresponding to when $h_{min} \sim \ell^3$) in Figure 11) the minima are *accelerating*; at later times (corresponding to when $h_{min} \sim \ell^6$ the minima are *decelerating*. As shown in Figure 14, the scaling laws for the velocities in the accelerating regime are given by $h_{min} \sim \dot{a}^{-6}$.

Let us now reexamine equation (13) governing the dynamics in the intermediate region. Solutions to (13) different from (14) result by assuming that a is

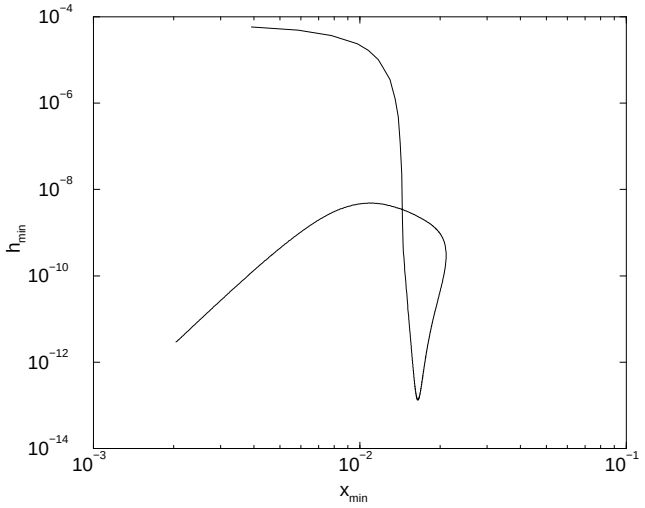

Figure 13: The minimum thickness h_{min} as a function of the minima locations $\pm x_{min}$, for the unstable exploding "singularity" of Figures 9 and 12. At $h_{min} \approx 10^{-13}$ the solution transitions to the imploding singularity.

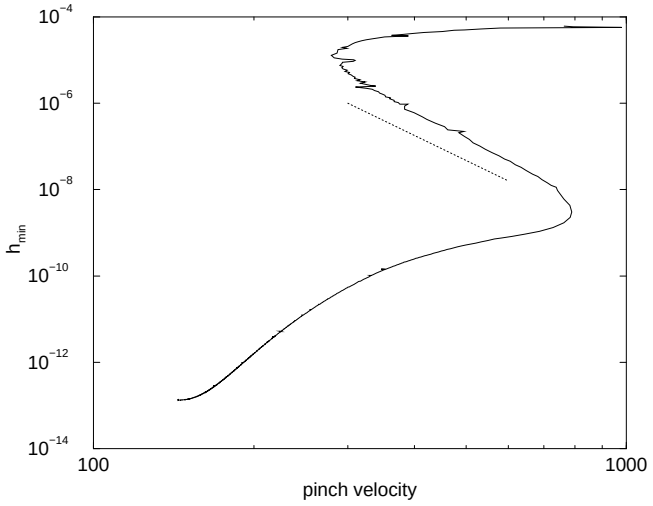

Figure 14: Minimum thickness h_{min} as a function of the velocity $\dot{a}$ of the pinch point, for the unstable exploding "singularity" of Figures 9 and 12. Note the presence of an accelerating and a decelerating regime. The dotted line represents the scaling law $h_{min} \sim \dot{a}^{-6}$.

not constant. These solutions obey the scaling laws

$$\begin{aligned} \dot{a} &\sim \ell^{r-3} \\ \ell &\sim (t_c - t)^{1/2} \\ \xi &\sim \frac{\ell^{r-1}}{\log \frac{\ell}{\xi}}. \end{aligned}$$

The only *a priori* requirement for the scaling exponent r is that the length scale ℓ in the intermediate region be much smaller than the length scale ξ governing the pinch region; this implies $r > 2$. The solution $r = 5/2$ has the scaling laws $\dot{a} \sim \ell^{-1/2}$, $h_{min} \sim \dot{a}^{-6}$, and $h_{min} \sim \ell^3$; this is consistent with the measured scaling laws for the accelerating intermediate region discussed in both this section and the preceding section. In the decelerating regime, Figure 11 shows that the outer intermediate length scale obeys the approximate scaling law $h_{min} \sim \ell^6$, suggesting $r = 4$ and $h_{min} \sim \dot{a}$. However, as observed above, Figure 14 shows a sharper decrease than this in the decelerating region, and might not even obey a strict power law.

This discrepancy suggests a possible mechanism for instability of the "exploding" similarity solution solution: the inner intermediate regions obeys a *different* scaling law than do the outer ones (see Figure 11). Denoting ℓ_i the outer intermediate length scale and ℓ_o the inner intermediate length scale, we have

$$\ell_i^7 \sim h_{min} \sim \ell_o^6$$

in the decelerating region. In the accelerating region, $h_{min} \sim \ell_o^3$, and ℓ_i decreases much more slowly with decreasing h_{min}.

Recall that the intermediate region dictates the time dependence of the singularity, as well as the velocity of the pinch point. The fact that there are different time dependences on the two sides of the pinch point means that the singularity is "frustrated:" should it move according to the directions of its left hand or its right?

A heuristic way of estimating when the instability will set in is as follows: We focus on the instability that occurs when the singularity is decelerating; a similar argument applies to the accelerating phase. The velocity of the pinch point dictated by the dynamics in the outer intermediate region is $\dot{a}_o \sim \ell_o^3$; the velocity of the pinch point dictated by the dynamics in the inner intermediate region is $\dot{a}_i \sim \ell_i^4$. When $a_o > a_i$, the dynamics of the outer flow pulls the minima outward. However, eventually there is a transition in which the inner flow has a stronger influence on the pinch points. At this point, the inner flow becomes more important, and the singularity becomes unstable. This heuristic argument suggests the instability criterion

$$\dot{a}_i \sim \dot{a}_o$$

or

$$\ell_i \sim \ell_o^{3/4}.$$

At the time of the instability shown above, $\ell_o \approx 4.66 \times 10^{-5}$ so the criterion predicts that the transition should occur when $\ell_i \approx 5.6 \times 10^{-4}$. This agrees quite well with the actual value of ℓ_i at the transition, $\ell_i \approx 1.38 \times 10^{-4}$. A similar argument applied to the instability of the accelerating singularity gives the same level of predictability.

In summary, we construct a one-parameter family of additional solutions governing the intermediate region; at special parameter values the solutions are observed in numerical simulations. The selection mechanism of these special parameters is not understood; moreover, it is apparent that the observed solutions have both have stable and unstable directions, as evidenced by initial convergence to the solutions followed by an instability. However, the constant velocity intermediate region appears to be robust, since we have never observed a transition away from the constant velocity solution. The stability and instability of these intermediate regions can be heuristically explained as a competition between the fluid in the inner and outer intermediate regions.

Before proceeding to the next section, we address how the instability threshold depends on the parameter w in the initial conditions. As the parameter w is increased toward $w_c \approx 0.0664$, the intermediate region converges to the constant velocity solution and a stable exploding singularity. For w below this threshold, there is always an instability. The minimum thickness at which the exploding similarity suffers the instability depends on the initial condition. Figure 15 shows how the turnaround thickness h_{trans} depends on w.

Near the critical value of $w_{crit} \approx 0.0664$, the critical thickness h_{trans} seems to approach zero. Near zero h_{trans} exhibits a power law as shown in Figure 16. A fit to the power law gives the scaling

$$h_{trans} \sim (w_c - w)^p \,,$$

with $p \approx 3.5$. An explanation of this power law behavior is currently lacking.

6 Symmetric Singularity

The third type of singular behavior resulting from the simple initial data (3) is the symmetric singularity. This type of scaling behavior results from initial data with w slightly larger than that producing the exploding singularity; an example of this solution for $w = 0.085$ is shown in Figure 17. The interface breaks at the origin after the finite time $t = 0.002547266$.

This singularity mechanism was first discovered by [BBDK94]. For equation (2) with $n < 1$, they constructed a similarity solution that well describes solutions from numerical simulations. However, their analysis breaks down for the case of present interest where $n = 1$; moreover, it was pointed out in [Ber95] that there is a second relevant length scale governing the singularity, neglected in the analysis of [BBDK94].

The present results clarify the situation considerably, although we still lack a complete theory for this type of singularity. We show below that there are both stable and unstable symmetric singularities. The pinch region for both of

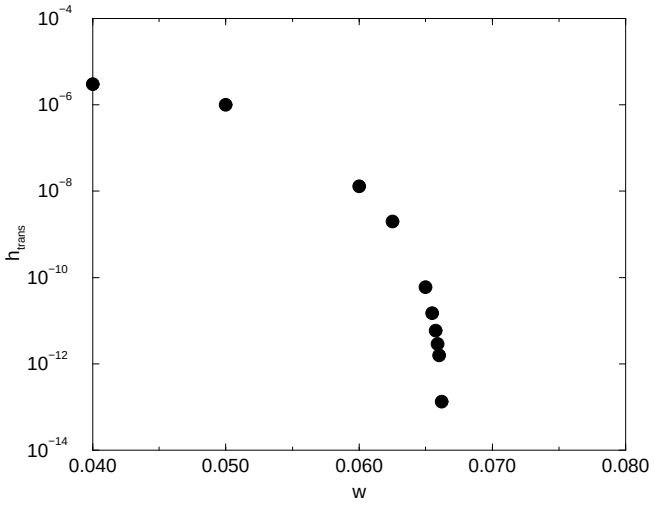

Figure 15: The thickness of the interface when the exploding singularity goes unstable as a function of the parameter w characterizing the initial conditions.

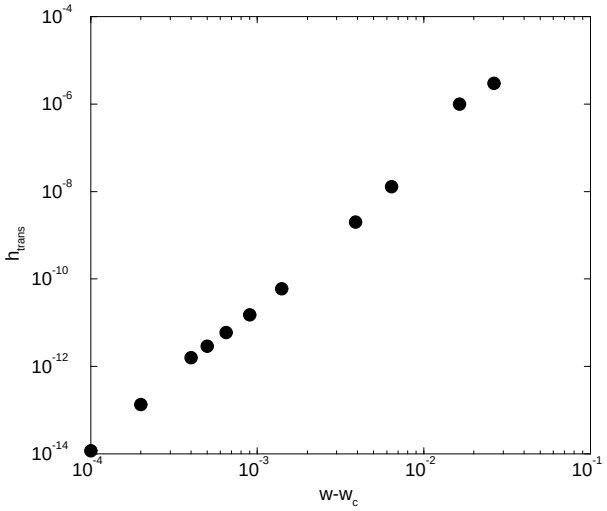

Figure 16: The thickness of the interface when the exploding singularity goes unstable as a function from the critical parameter $w_c = 0.0664$.

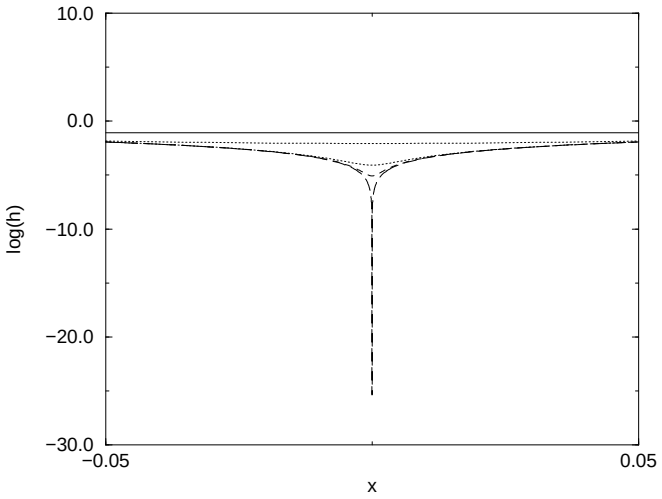

Figure 17: Symmetric singularity formation for $w = 0.085$. The neck of fluid breaks in the center, symmetrically about the pinch point.

these solutions has a spatial dependence similar to that proposed by [BBDK94] for equation (2) with $n < 1$, although the time dependence is more complicated. The *stable* symmetric singularity is demonstrated to have an intermediate length scale, with a nontrivial scaling law. The *unstable* symmetric singularity, on the other hand, appears to be governed by a single length scale throughout. We show that these behaviors in the intermediate region lead to destabilization of the pinch region scaling followed by breakup of this singularity structure.

6.1 The Pinch Region

The solution in the pinch region is of the form

$$h(x,t) \;=\; \delta(\xi)\left(1+\tfrac{1}{2}\eta^2\right) \;+\; \gamma(\xi)\,G(\eta) \;+\; \ldots. \tag{16}$$

Here $\xi(t)$ is a characteristic length scale, which goes to zero as the singularity occurs, and $\delta(\xi)$ denotes the local minimum of the solution. The variable $\eta = x/\xi$ is the similarity space variable. The expansion in (16) is in powers of ξ; we have neglected terms of order $\gamma\xi$, which are smaller than the ones written for the range of interest $\eta \lesssim \mathcal{O}(1)$.

Plugging (16) into (1) gives

$$-\dot{\xi}\left[\delta' + \left(\delta' - \frac{2\delta}{\xi}\right)\tfrac{1}{2}\eta^2 + \gamma' G - \frac{\gamma}{\xi}\eta G_\eta + \ldots\right] = \\ = \frac{\gamma}{\xi^4}\left[\left(\delta\left(1+\tfrac{1}{2}\eta^2\right) + \gamma G + \ldots\right)\left(G_{\eta\eta\eta} + \ldots\right)\right]_\eta \quad (17)$$

($-\dot{\xi} > 0$ since ξ is decreasing). We now compute the function $G(\eta)$, which gives the leading order correction to the parabolic shape, for small ξ. To do this, we must identify the dominant terms on each side of (17).

For Eq. (2) with $n < 1$ [BBDK94], such symmetric singularities occur with $\delta \sim \xi^2$, for which $\delta' - 2\delta/\xi = 0$. For $n = 1$, logarithmic-type corrections appear: our numerics suggest that $\delta \sim \xi^2 P(\log\xi)$, where P has at most polynomial growth at infinity. Then $\delta' - 2\delta/\xi = \xi\, P'(\log\xi)$, which is smaller than δ' by a factor of $\log\xi$. We therefore argue that the dominant term is the leading one, $-\dot{\xi}\delta'$, and we look for a consistent balance under this assumption.

On the right-hand side, the leading term is the first one, $\gamma\xi^{-4}\,\delta\left(1+\frac{1}{2}\eta^2\right)G_{\eta\eta\eta}$. Balancing the dominant terms, and separating variables for the two dependences on ξ and η, we determine both

$$G_{\eta\eta\eta} = \frac{\eta}{1+\frac{1}{2}\eta^2}, \quad \text{and} \quad \gamma = -\frac{\xi^4\dot{\xi}\,\delta'}{\delta}.$$

Figure 18 shows excellent agreement of the numerics with this similarity solution. The rescaled data has h_{min} ranging from 10^{-5} to 10^{-35}. The rescaling uses the maximum of h_{xxx} as a rescaling parameter.

Although we have found the correct functional form for the spatial dependence in the pinch region, we have not determined the time dependence of the solution. As in the exploding singularity above it is natural to imagine that the time dependence might occur as a matching condition to an intermediate region.

6.2 Intermediate Region

Indeed, the symmetric singularity for $w = 0.85$ also has structure on an intermediate length scale ℓ, which is much larger than ξ. The existence of this intermediate scale was first pointed out in [Ber95] for the forced Hele-Shaw cell as the length scale over which $\partial_t h$ varies.

Figure 19 shows the minimum thickness as a function of both this intermediate length scale and the pinch region length scale (defined as above as the length scale over which h varies), for the initial condition $w = 0.085$ shown above.

The data suggests the scaling laws

$$h_{min} \;\sim\; \xi^2 \;\sim\; \ell^{2.5}.$$

There is a clear difference in size between the intermediate scale and the pinch scale, with the intermediate scale always much larger than the pinch scale. Measuring the intermediate scale as a function of time gives a power law consistent with $\ell \sim (t_c - t)^{0.5}$.

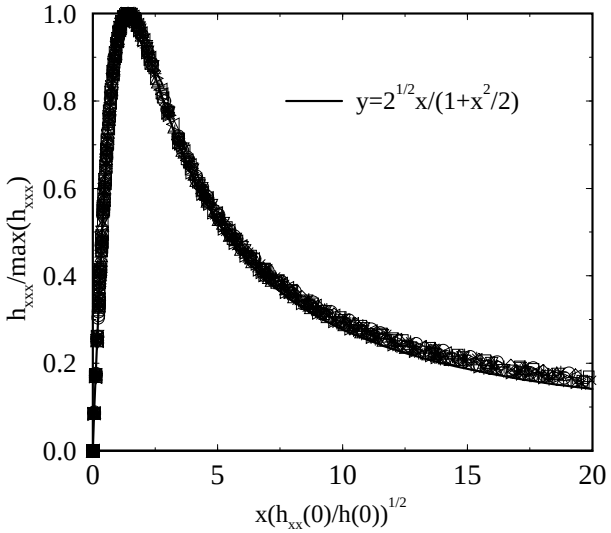

Figure 18: Rescaled third derivative for approximately 15 decades in the characteristic width ξ.

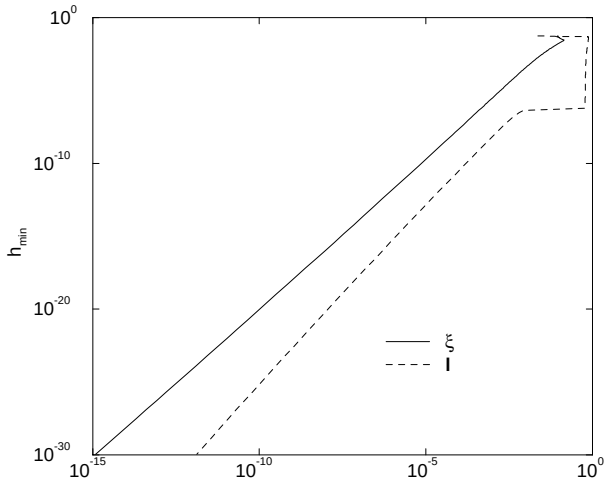

Figure 19: Minimum thickness h_{min} as a function of both the intermediate length scale ℓ and the pinch length scale ξ, measured as described in the text.

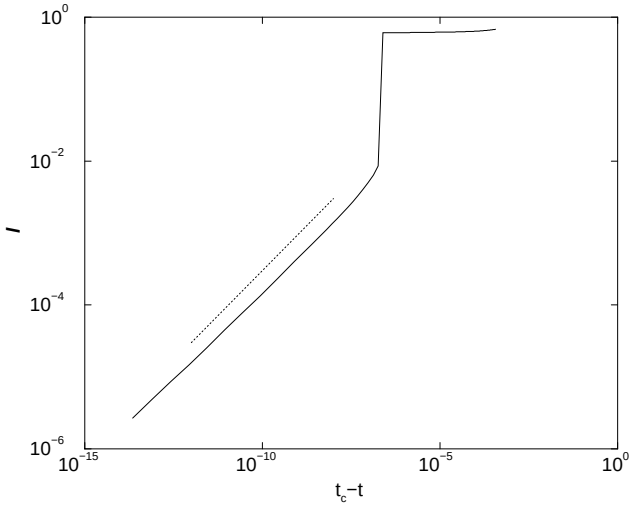

Figure 20: The characteristic length scale in the intermediate region as a function of the time to the singularity, $t_c - t$. The dotted line shows the scaling law $\ell \sim (t_c - t)^{0.5}$.

6.3 Destabilization of the Solution

Thus far we have presented numerical evidence for the existence of a locally symmetric singularity. The simulation described above shows over ten decades of scaling in the characteristic width of the solution. However, for slightly lower values of the parameter w, the symmetric singularity becomes unstable. As in the case of the "exploding" singularity instability described in the preceding section, this instability can set in at an arbitrarily small thickness, depending on the initial data. We illustrate the instability using initial data with $w = 0.08$ (see Figure 21).

At early times (the uppermost curve) the solution falls by ten orders of magnitude, and seems to approach the symmetric singularity. However, the solution eventually bifurcates into an exploding singularity, with two minima.

Evidence of the impending breakdown of the symmetric scaling structure can be found well before it occurs in both the intermediate region and the pinch region. Plotting the minimum thickness as a function of the intermediate length scale and the pinch scale tells a dramatically different story from the stable symmetric singularity discussed above. Figure 22 shows that the intermediate scale and the pinch scale have essentially identical scaling laws (up to possible logarithmic corrections). In fact, the intermediate scale seems to have a slightly steeper slope. The instability occurs exactly when the characteristic scale of the pinch region is equal to the characteristic scale of the intermediate region,

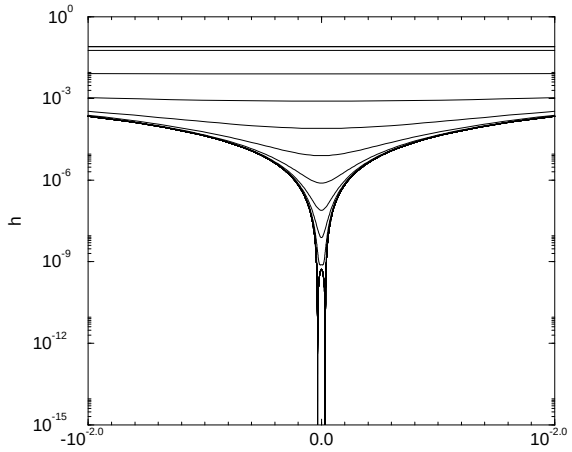

Figure 21: Destabilization of the symmetric singularity for $w = 0.08$. The uppermost curve corresponds to the earliest time, and the lower-most curve corresponds to the latest time. Although the thickness at the origin initially falls by almost ten orders of magnitude, this "symmetric singularity" eventually bifurcates into an exploding singularity, with two minima.

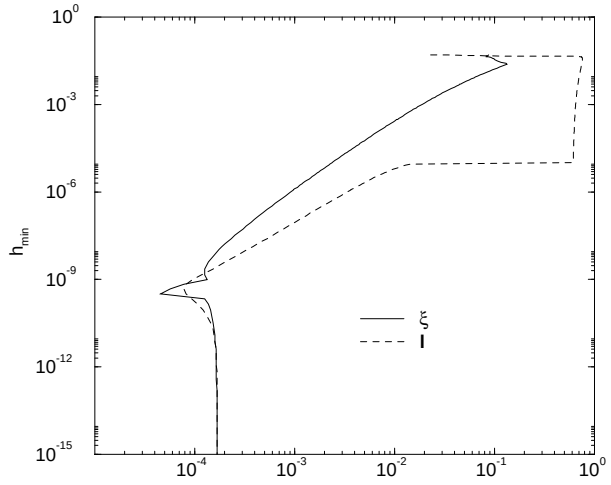

Figure 22: Intermediate length scale ℓ (dashed line) and pinch length scale ξ (solid line) plotted against minimum thickness h_{min}.

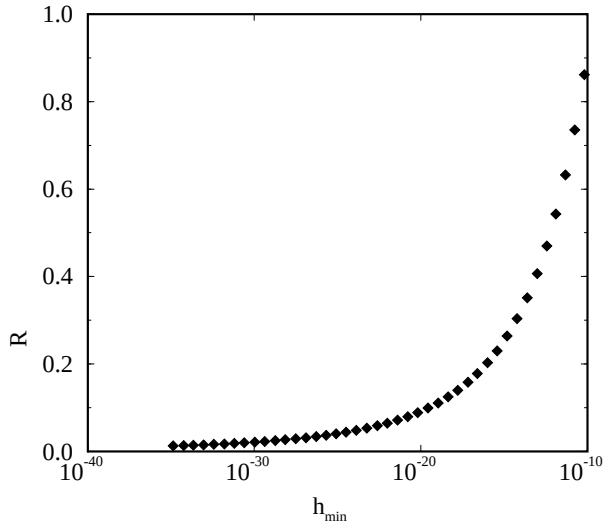

Figure 23: Plot of R as a function of h_{min} for the stable symmetric singularity at $w = 0.085$. The ratio decreases monotonically as $h_{min} \to 0$.

$\xi \sim \ell$.

The instability can also be predicted by studying the properties of the solution in the pinch region. In the above analysis of the pinch region, we computed the first two terms in an expansion and showed that the second term has size

$$\gamma = \frac{\dot{\xi}\delta'\xi^4}{\delta}.$$

In order for this term to be lower order than the first term, of size δ, the ratio $R = \gamma/\delta$ must be small compared with 1. Figure 23 shows R versus h_{min} for the stable symmetric singularity.

On the other hand, in the case where the singularity destabilized, R initially decreases but then starts to increase very slowly (Figure 24). A rapid rise in R then precedes the destabilization right before bifurcation of the minimum occurs (Figure 25).

The fact that the unstable symmetric singularity and the stable symmetric singularity have different time dependences of R and different intermediate regions in the two cases indicates that we are observing two different singular solutions of the PDE. Thus far we have not been able to construct an entirely convincing similarity solution that recovers the scaling properties of either of the two cases.

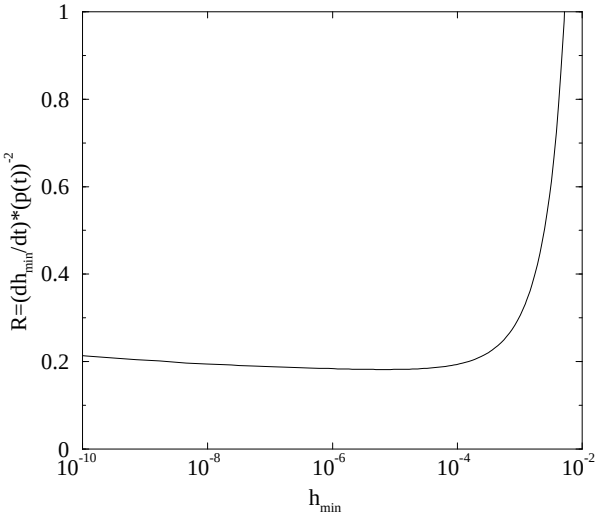

Figure 24: Plot of R as a function of h_{min} for the unstable symmetric singularity at $w = 0.08$. In this case the ratio grows very slowly as $h_{min} \to 0$, again with a logarithmic time dependence.

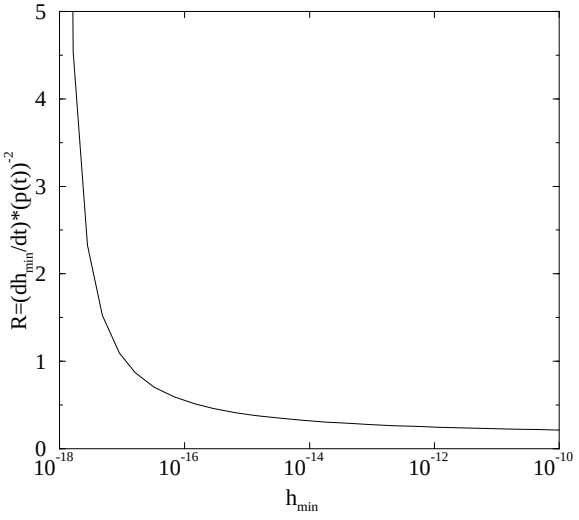

Figure 25: Plot of R as a function of h_{min} for the unstable symmetric singularity at $w = 0.08$. The figure shows a closeup of the sharp increase right before bifurcation occurs.

7 Conclusions

This paper describes a set of complex phenomena associated with scaling and singularity formation in a thin neck in the unforced Hele-Shaw cell. We show several types of possible behavior associated with singularity formation, two of which appear in previous work on the forced Hele-Shaw cell. We support the evidence presented in the numerical simulations by constructing self-similar local solutions to the governing equations that agree with the numerics; taken together these results provide convincing evidence that there are several different mechanisms for the formation of finite time singularities.

We emphasize that the observation of *multiple* similarity solutions depending on the details of the initial conditions and boundary conditions is quite different from other physical situations. All of the similarity solutions in the Hele-Shaw problem have scaling exponents unrelated to dimensional analysis; this is in stark contrast to three-dimensional droplet breakup, where there is a single similarity solution with dimensional exponents. The existence of so many different similarity solutions is interesting because it means that arguments about universality of the singularity become vacuous: slight changes in initial conditions and boundary conditions *can* influence the singular behavior, even though the singularity happens on a time scale arbitrarily faster than the boundary forcing.

A particularly intriguing result of the present work is the observation that similarity solutions can apparently destabilize at arbitrarily small thickness, with the thickness at which instability occurs depending on the initial condition. Before the instability sets in, arbitrarily many decades of scaling can occur. It is important to note that less well resolved numerics would miss the instabilities and therefore provide an inaccurate description of the singularity behavior. Instabilities have been previously observed in similarity solutions characterizing three dimensional axisymmetric droplet breakup [BSN94, SBN94]; however in that case the instabilities are manifestations of the Rayleigh instability, which is absent in the our two dimensional system. The instabilities observed here are more subtle, and a complete understanding would require stability analysis of the different matching regions.

The existence of unstable similarity solutions highlights our current lack of understanding of the selection of scaling solutions near singularities. What causes the selection of a particular singular behavior? Does the selection depend on boundary conditions? Although stability analysis of a single similarity solution with a well defined asymptotic behavior is straightforward (see for example [BSN94]), it is unknown how to perform stability analysis when there are several matching regions with different time dependences. Even more important, the time dependences are always determined by assuming a certain asymptotic behavior away from the singularity; we do not know what determines the particular asymptotic behavior selected. Without understanding these issues, we cannot rule out that *any* of the singular behaviors described to date in the Hele-Shaw cell (or for that matter in any system where singularities form) may be inherently unstable. For example, we do not observe instabilities of the con-

stant velocity exploding singularity; however, this apparent stability could be a remnant of our finite numerical resolution.

Many computational studies address scaling properties of singularities. In more complex equations such as 3D Euler, one can only resolve a few decades of scaling with current computational technology [Ker93]. It may be that such destabilizations also occur in systems like this yet the numerical tools are not refined enough to observe them. Our study shows that numerical calculations of finite time singularities, even when many decades of scaling are present, may not show the true end state of the system. We emphasize that this is even true when the calculations are resolved well below all important physical length scales, as instabilities can occur on scales determined by intermediate matching regions, which can be arbitrarily small.

Another fundamental question reiterated by this study is why are the singularities of the lubrication approximation (1) not described by exact similarity solutions, predicted by dimensional analysis? In three dimensional droplet breakup, such dimensional similarity solutions are relevant [Egg93, SBN94] for understanding rupture. However, although we have uncovered at least six different similarity solutions observed (either transiently or asymptotically) in the simulations, none of them are exact similarity solutions.

Finally, we end with a plea to experimentalists: Other than the initial experiments that prompted studies of droplet breakup in a Hele-Shaw cell [GMS], no systematic experimental investigations have been carried out. The main reason that such experiments are difficult because of the need to resolve a large range of scales to test the detailed predictions and scaling laws. In a typical Hele-Shaw experiment, the plate spacing b is around 1 mm, which in the best of circumstances could give only a decade of scaling, hardly sufficient to test theoretical predictions. However, the present results suggest that there are *qualitative* predictions that would be both worthwhile and possible to test experimentally: we suggest that it should be experimentally feasible to tune between the different similarity solutions. Since the different singular behaviors have different qualitative features (e.g. finite time versus infinite time, stationary pinch point versus moving pinch point, symmetric versus asymmetric, imploding versus exploding). Their qualitative features will be easily distinguishable, even by the number of satellite drops that are left by this most interesting topological transition.

Acknowledgments

We thank Leo Kadanoff, Todd Dupont, and Peter Constantin for discussions and encouragement. This research was partially supported by the MRSEC Program of the National Science Foundation under Award Number DMR-9400379. In addition, R.A. is partially supported by an Alfred P. Sloan Foundation Research Fellowship, and A.B. is supported by Office of Naval Research grant N00014-95-1-0752 and the Mathematical, Information, and Computational Sciences Division subprogram of the Office of Computational and Technology Research, U.S. Department of Energy, under Contract W-31-109-Eng-38. M.B.

acknowledges an NSF postdoctoral fellowship.

References

[Alm96] Robert Almgren. Singularity formation in Hele-Shaw bubbles. *Physics of Fluids*, 1996. To appear.

[Bar79] G. I. Barenblatt. *Similarity, Self-Similiarity, and Intermediate Asymptotics*. Consultant's Bureau, Plenum Publishing Corp., New York, 1979.

[BBDK94] Andrea L. Bertozzi, Michael P. Brenner, Todd F. Dupont, and Leo P. Kadanoff. Singularities and similarities in interface flows. In Lawrence Sirovich, editor, *Trends and Perspectives in Applied Mathematics*, pages 155–208. Springer-Verlag, 1994.

[Ber95] Andrea L. Bertozzi. Symmetric singularity formation in lubrication-type equations for interface motion. *SIAM J. Appl. Math.*, 1995. To appear.

[BKL+86] David Bensimon, Leo P. Kadanoff, Shoudan Liang, Boris I. Shraiman, and Chao Tang. Viscous flows in two dimensions. *Rev. Mod. Phys.*, 58:977–999, 1986.

[BKO93] Stefanella Boatto, Leo P. Kadanoff, and Piero Olla. Traveling-wave solutions to thin-film equations. *Phys. Rev. E*, 48:4423–4431, 1993.

[BP95] A. L. Bertozzi and M. Pugh. The lubrication approximation for thin viscous films: Regularity and long time behavior of weak solutions. *Comm. Pure Appl. Math.*, 1995. To appear.

[BSN94] Michael P. Brenner, X. D. Shi, and Sidney R. Nagel. Iterated instabilities during droplet fission. *Phys. Rev. Lett.*, 73:3391–3394, 1994.

[CDG+93] Peter Constantin, Todd F. Dupont, Raymond E. Goldstein, Leo P. Kadanoff, Michael Shelley, and Su-Min Zhou. Droplet breakup in a model of the Hele-Shaw cell. *Phys. Rev. E*, 47:4169–4181, 1993.

[CP93a] Russel E. Caflisch and George C. Papanicolaou. *Singularities in Fluids, Plasmas, and Optics*, volume C404 of *NATO ASI Series*. Kluwer Academic Publishers, 1993.

[CP93b] P. Constantin and M. Pugh. Global solutions for small data to the Hele-Shaw problem. *Nonlinearity*, 6:393–415, 1993.

[DGKZ93] Todd Dupont, Raymond Goldstein, Leo Kadanoff, and Su-Min Zhou. Finite-time singularity formation in Hele-Shaw systems. *Phys. Rev. E*, 47:4182–4196, 1993.

[ED94] Jens Eggers and Todd F. Dupont. Drop formation in a one-dimensional approximation of the Navier-Stokes equation. *J. Fluid Mech.*, 262:205, 1994.

[Egg93] Jens Eggers. Universal pinching of 3D axisymmetric free-surface flow. *Phys. Rev. Lett.*, 71:3458–3460, 1993.

[GMS] R. E. Goldstein, T. G. Mason, and E. Shyamsunder. Private communication.

[GPS93] Raymond E. Goldstein, Adriana I. Pesci, and Michael J. Shelley. Topology transitions and singularities in viscous flows. *Phys. Rev. Lett.*, 70:3043–3046, 1993.

[GPS95] Raymond E. Goldstein, Adriana I. Pesci, and Michael J. Shelley. Preprint, 1995.

[Ker93] Robert M. Kerr. Evidence for a singularity of the three-dimensional, incompressible Euler equations. *Phys. Fluids*, 5:1725–1746, 1993.

[KKL88] David A. Kessler, Joel Koplik, and Herbert Levine. Pattern selection in fingered growth phenomena. *Advances in Physics*, 37:255–339, 1988.

[Lew94] M. A. Lewis. Spatial coupling of plant and herbivore dynamics: the contribution of herbivore dispersal to transient and persistent "waves" of damage. *Theoretical Population Biology*, 45, 1994.

[Maj86] A. J. Majda. Vorticity and the mathematical theory of incompressible fluid flow. *Comm. Pure Appl. Math.*, 39:5187–5220, 1986.

[PS92] A. Pumir and E. D. Siggia. Development of singular solutions to the axisymmetric Euler equations. *Phys. Rev. Lett.*, 68:1511–1514, 1992.

[SBN94] X. D. Shi, M. P. Brenner, and S. R. Nagel. A cascade of structure in a drop falling from a faucet. *Science*, 265:219–222, 1994.

[VMBM88] P. W. Voorhees, G. B. McFadden, R. F. Boisvert, and D. I. Meiron. Numerical simulation of morphological development during Ostwald ripening. *Acta Metall.*, 36:207–222, 1988.

List of Figures